Available online at www.sciencedirect.com

SciVerse ScienceDirect

Ceramics International 38 (2012) 2403–2409

CERAMICS INTERNATIONAL

www.elsevier.com/locate/ceramint

Electrolyte materials for solid oxide fuel cells derived from metal complexes: Gadolinia-doped ceria

Chatchai Veranitisagul [a,b], Attaphon Kaewvilai [c,d], Worawat Wattanathana [e], Nattamon Koonsaeng [e], Enrico Traversa [a,f], Apirat Laobuthee [c,d,*]

[a] Department of Chemical Science and Technology, University of Rome "Tor Vergata", Rome 00133, Italy

[b] Department of Materials and Metallurgical Engineering, Faculty of Engineering, Rajamangala University of Technology Thanyaburi, Thanyaburi, Pathumthani 12110, Thailand

[c] Department of Materials Engineering, Faculty of Engineering, Kasetsart University, Chatuchak, Bangkok 10900, Thailand

[d] Center of Advanced Studies in Industrial Technology, Faculty of Engineering, Kasetsart University, Chatuchak, Bangkok 10900, Thailand

[e] Department of Chemistry, Faculty of Science, Kasetsart University, Chatuchak, Bangkok 10900, Thailand

[f] International Research Center for Materials Nanoarchitectonics (MANA), National Institute for Materials Science (NIMS), Tsukuba, Ibaraki 305-0044, Japan

Received 5 August 2011; received in revised form 2 November 2011; accepted 2 November 2011

Available online 7 November 2011

Abstract

Gadolinia doped ceria (GDC) powders with different gadolinium contents were successfully prepared by the thermal decomposition of ceria complexes. All the calcined powder samples were found to be ceria-based solid-solutions having a fluorite-type structure. The powders were cold-isostatically pressed and sintered in air at 1500 °C for 5 h to attain a sintered density of about 90% of its theoretical value. The electrical conductivity of the GDC pellets in air was studied as a function of temperature in the 225–700 °C range, by using two-probe electrochemical impedance spectroscopy measurements. The highest total conductivity ($\sigma_{600\ °C}$ = 0.025 S/cm) was found for the $Ce_{0.85}Gd_{0.15}O_{1.925}$ composition.

Keywords: A. Powders: chemical preparation; C. Ionic conductivity; D. CeO_2; E. Fuel cells

1. Introduction

Solid oxide fuel cells (SOFCs) using oxygen-ion conducting electrolytes offer a low-pollution technology to directly convert chemical energy into electricity with high efficiency [1]. The advantages of SOFCs over other conventional energy conversion systems include high efficiency, modularity, fuel adaptability, and very low levels of emissions depending on the fuel used [2]. However, SOFC operation needs elevated temperatures, above 900 °C, due to the use of yttria-stabilized zirconia (YSZ) as the electrolyte material, which results in high costs and in decreasing the durability, due to electrode sintering and interfacial reactions. Improved durability, a wider choice for interconnecting material selection, and lower costs can be achieved by reducing the operating temperature below 700 °C [3].

For this purpose, electrolytes with high oxygen-ion conductivity at low temperatures are under investigation. Moreover, reducing the electrolyte thickness decreases the electrolyte ohmic resistance. Gadolinia-doped ceria (GDC) is an attractive electrolyte alternative to YSZ, owing to its superior oxygen ion conductivity at low temperatures [4,5]. Ceria doping is needed to increase the oxygen vacancy concentration and to reduce the intrinsic electronic conductivity. Among the various doping elements investigated, Gd^{3+} and Sm^{3+} doped ceria (GDC and SDC) were reported to have the largest conductivity [6]. Moreover, studies have been carried out on co-doped ceria [7–10].

Currently, the common synthesis routes to prepare doped ceria powders include solid-state reaction [11,12], co-precipitation reaction [12–15], hydrothermal synthesis [16] and sol–gel routes [17]. However, these synthesis routes have some

* Corresponding author at: Department of Materials Engineering, Faculty of Engineering, Kasetsart University, Chatuchak, Bangkok 10900, Thailand. Tel.: +66 2 942 8555x2132; fax: +66 2 955 1811.

E-mail address: fengapl@ku.ac.th (A. Laobuthee).

0272-8842/$36.00
doi:10.1016/j.ceramint.2011.11.006

disadvantages, such as the cost of the starting materials, complexity, slowness, lack of homogeneity and purity, and high processing temperature. SOFC electrolyte materials usually possess complex compositions with several metallic elements, and therefore selecting a simple and low-cost method to effectively prepare doped ceria powders has distinct advantages for SOFC research.

In a previous work, Laobuthee et al. used a simple and straightforward method to directly prepare Mg–Al–TEA complex from $Al(OH)_3$, MgO and triethanolamine (TEA), as a precursor for magnesium aluminate spinel ($MgAl_2O_4$) via the oxide one pot synthesis (OOPS) process [18]. The obtained $MgAl_2O_4$, exhibiting high purity and homogeneity, was tested as a humidity sensor material [18]. However, this method showed some disadvantages, such as the limited solubility of the starting materials, the high boiling point of the ethylene glycol solvent, and the required reaction temperature at 200 °C. To address these limitations, based on the OOPS process, the nitrate salts were alternatively used as starting materials. Lower boiling point solvents, such as propan-1-ol and butan-1-ol, were also used to replace ethylene glycol. The complexes prepared by modified method were used as precursors for the production of high quality GDC powders, which were sintered into pellets and then characterized their electrochemical properties.

2. Experimental

The starting materials were cerium(III) nitrate hexahydrate [$Ce(NO_3)_3{\cdot}6H_2O$, 99.5% purity] and gadolinium(III) nitrate pentahydrate [$Gd(NO_3)_3{\cdot}5H_2O$, 99.9% purity], purchased from Acros Organics. Triethanolamine [TEA, $N(CH_2CH_2OH)_3$, 98% purity] and propan-1-ol [$CH_3CH_2CH_2OH$, 99.5% purity] were obtained from Carlo Erba (Barcelona). All chemicals were used as provided.

The complexes were prepared by mixing in 80 mL propan-1-ol, $Ce(NO_3)_3{\cdot}6H_2O$ and $Gd(NO_3)_3{\cdot}5H_2O$, with the molar ratios of Ce:Gd = 0.9:0.1, 0.85:0.15, and 0.8:0.2, denoted $Ce_{0.9}Gd_{0.1}O_{1.95}$, $Ce_{0.85}Gd_{0.15}O_{1.925}$, and $Ce_{0.8}Gd_{0.2}O_{1.9}$, respectively. TEA was added in the 1:1 molar ratio of metal ions to TEA. After amalgamation, the as-prepared transparent solutions were distilled for 3 h in order to obtain the complex precipitates. The precipitates were collected by filtration and then washed with propan-1-ol. Simultaneous thermogravimetric and differential thermal analysis (TG/DTA) of the complexes was performed using a TGA/SDTA analyzer (Model TGA/SDTA 851e, Mettler Toledo), in flowing air with a heating rate of 5 °C/min, in the 50–1000 °C temperature range.

The complexes were calcined in an alumina crucible at various temperatures: 400, 600, 800, 1000, and 1200 °C for 2 h. Phase identification was performed using X-ray diffraction analysis (XRD; Philips X-Pert-MPD X-ray diffractometer) operating at 40 kV/30 mA, with monochromated Cu Kα radiation. Diffraction patterns were recorded in the range of $2\theta = 20–90°$ by step-scanning, with a step interval of 0.02° and a scanning time of 2 s for each step.

The specific surface area of the powders, S_{BET}, was measured using the Brunauer–Emmett–Teller (BET) nitrogen-gas absorption method. The values were calculated from the nitrogen absorption isotherms at 77 K, using a Micromeritics ASAP 2020 surface analyzer at a value of 0.162 nm^2 for the cross-section of the nitrogen molecule. Samples were degassed at 350 °C under high vacuum conditions for 20 h before measurements. The specific surface area was converted to particle size (D_{BET}) according to Eq. (1), under the approximation that the particles were closed spheres with a smooth surface and of uniform size.

$$D_{BET} = \frac{6 \times 10^3}{d_{th} S_{BET}} \quad (1)$$

Here, d_{th} was the theoretical density of the material (g/cm^3) and D_{BET} was the average particle size (nm). The specific surface area, S_{BET}, was expressed in m^2/g.

Scanning electron micrographs were obtained using a JEOL JSM-6301F scanning electron microscope (SEM) operating at an acceleration voltage of 12 kV, to identify the powder microstructure. Samples were mounted on aluminum stubs using carbon tape and then sputter coated with Au to avoid particle charging.

The obtained powders were uniaxially pressed into green pellets (~30 MPa) in a stainless steel die of 10 mm in diameter, and then isostatically pressed at ~200 MPa. When not specified, the powders used were those calcined at 600 °C. Dense pellets were prepared by sintering the green pellets at 1500 °C for 5 h with a ramp rate of 3 °C/min and naturally cooled in the furnace. The relative density of the sintered pellets was determined using the Archimedes' principle. Powder XRD analysis was performed on polished samples.

Electrodes were painted using a gold paste onto both sides of the pellets, and fired at 800 °C for 2 h. The pellets were placed in an alumina holder using a spring-clip arrangement between Pt current collectors. The electrochemical impedance spectroscopy (EIS) measurements were performed from 0.1 Hz to 10 MHz, using a Solartron 1260 impedance/gain phase analyzer, interfaced to a personal computer, and run through ZPlot® and Zview software (Scribner Associates, Incorporated); 10 points were taken per decade of frequency. The amplitude of the AC signal imposed on the samples was 10 mV. The EIS measurements were performed at controlled temperatures in the 225–700 °C range.

3. Results and discussion

The various complexes between $Ce(NO_3)_3$, $Gd(NO_3)_3$, and TEA were prepared in propan-1-ol. Yellowish powders were obtained, although the contents of Ce^{3+} and Gd^{3+} varied. The yellowish powders were precipitated when the complexes completely reacted in propan-1-ol for 3 h.

To obtain the ceramic powders, the complexes were calcined to remove the organic contents. The appropriate temperature for calcination was studied using TG/DTA measurements. Fig. 1, as an example, shows the TG/DTA curves of the complex for 10 mol% GDC. The broad endothermic peak, centered at ~100 °C on the DTA curve, was mainly caused by the loss of

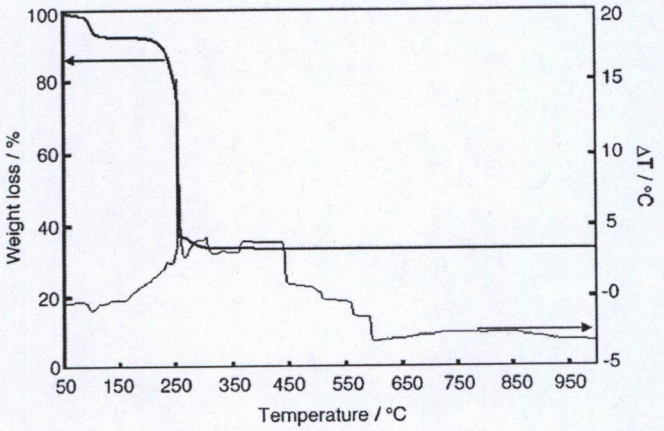

Fig. 1. TG and DTA curves of a 10 mol% doped gadolinium CeO_2 complex.

Table 1
Specific surface area (S_{BET}) and average particle size (D_{BET}) of $Ce_{0.9}Gd_{0.1}O_{1.95}$, $Ce_{0.85}Gd_{0.15}O_{1.925}$, and $Ce_{0.8}Gd_{0.2}O_{1.9}$ powders calcined at various temperatures.

Sample	T (°C)	Specific surface area, S_{BET} (m^2/g)	D_{BET} (nm)
$Ce_{0.9}Gd_{0.1}O_{1.95}$	600	23.6	35
	800	19.2	43
	1000	7.5	111
$Ce_{0.85}Gd_{0.15}O_{1.925}$	600	28.6	29
	800	15.0	55
	1000	7.8	106
$Ce_{0.8}Gd_{0.2}O_{1.9}$	600	22.1	38
	800	12.9	65
	1000	8.6	97

physisorbed water and propan-1-ol. The sharp exothermic peak with its maximum at 250 °C, accompanied by an abrupt weight loss in the TG curve, was caused by the decomposition of the organic ligand and generated char as a by-product. A slight weight loss together with broad exothermic effects was observed in the 300–600 °C temperature range, which was ascribed to the burning of the residual organic components. Above 600 °C, no weight loss was observed, showing that the appropriate calcination temperature for the preparation of the ceramic powders is likely to be 600 °C.

Based on the TG/DTA analysis, the complexes were calcined at 400, 600, 800, 1000 and 1200 °C for 2 h in air. The obtained products were light-yellowish colored powders. XRD was used to characterize the powders. Fig. 2 shows the XRD patterns of the $Ce_{0.8}Gd_{0.2}O_{1.9}$ powders at various heating temperatures. Before calcination, all the complexes exhibited low crystallinity. In agreement with the results of TG/DTA analysis, the powders of each complex calcined at 600 °C for

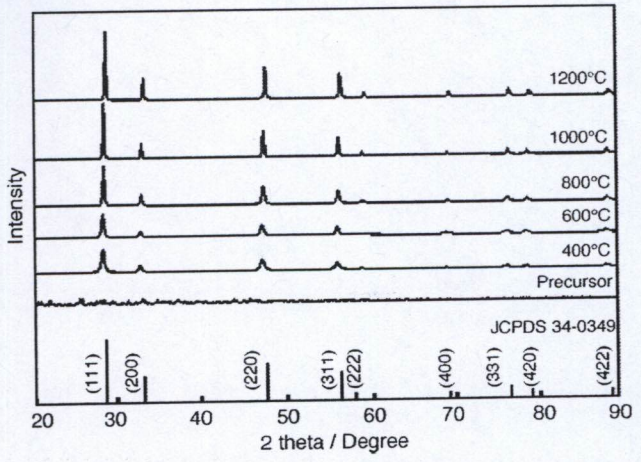

Fig. 2. XRD patterns of the 20 mol% doped gadolinium CeO_2 complex and $Ce_{0.8}Gd_{0.2}O_{1.9}$ powders calcined between 400 and 1200 °C.

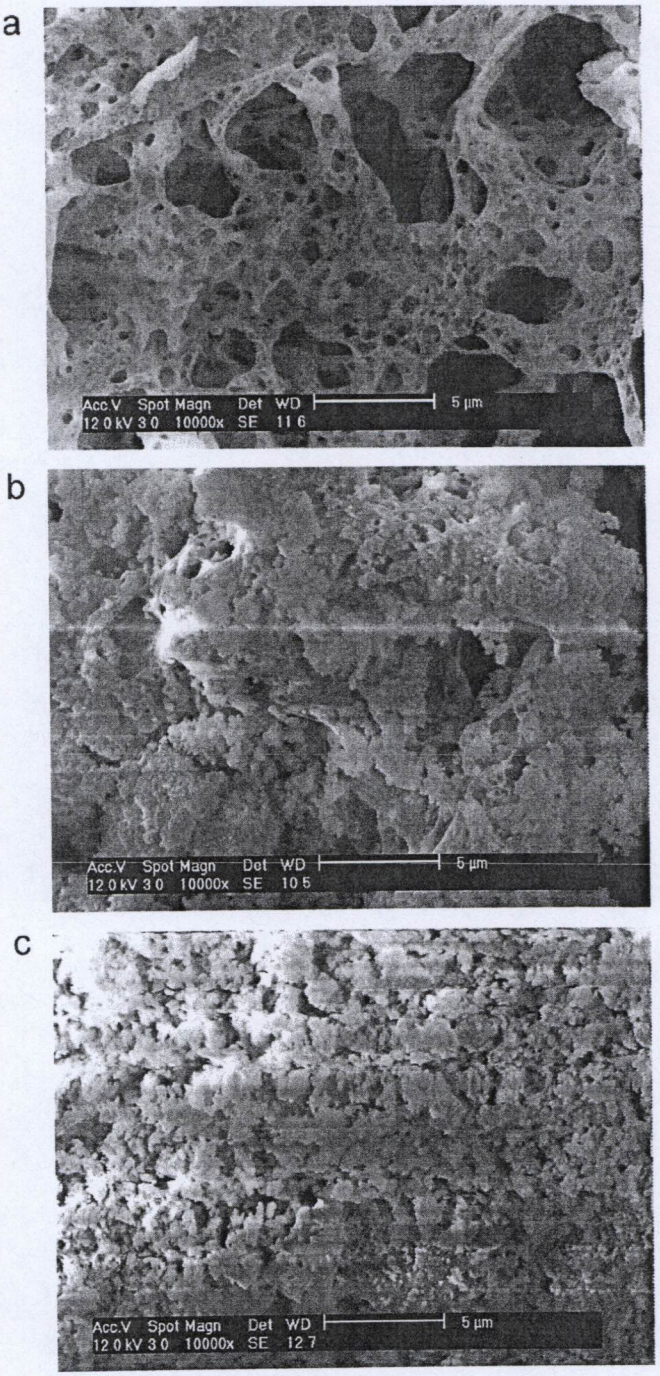

Fig. 3. SEM micrographs of the $Ce_{0.8}Gd_{0.2}O_{1.9}$ powder calcined at (a) 600 °C, (b) 800 °C and (c) 1000 °C.

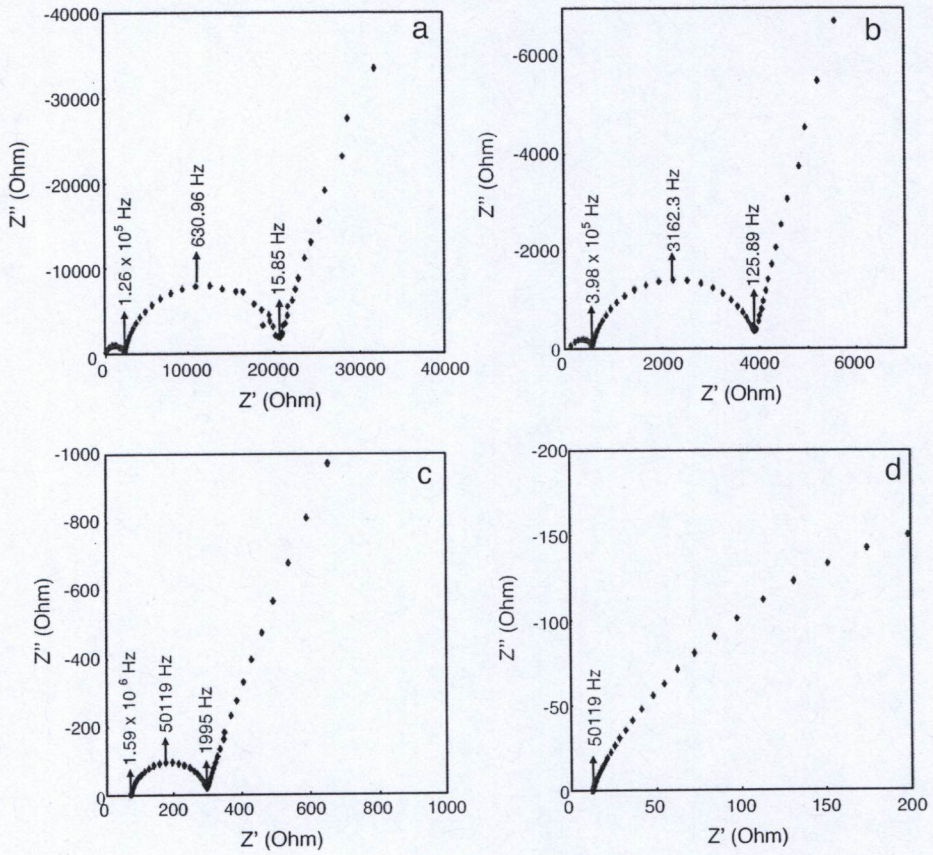

Fig. 4. Complex impedance plane plots of $Ce_{0.85}Gd_{0.15}O_{1.925}$ pellet sintered at 1500 °C, measured at (a) 250 °C, (b) 300 °C, (c) 400 °C and (d) 600 °C in air.

2 h displayed only reflections corresponding to the fluorite structure of CeO_2 (JCPDS Powder Diffraction File No. 34-0394). The diffraction peaks of each powder sample were sharper and narrower with increasing the heating temperature, indicating an increase in the crystallite size. The same trend was also observed for the $Ce_{0.9}Gd_{0.1}O_{1.95}$ and $Ce_{0.85}Gd_{0.15}O_{1.925}$ samples. No crystalline phases corresponding to Gd_2O_3 could be found at any calcination temperatures for the Gd-doped complexes, showing the direct formation of solid solutions.

Table 1 summarizes the specific surface area values obtained for the calcined powders. Table 1 also reports the average particle size (D_{BET}) of the powders calcined at 600, 800, and 1000 °C, which were calculated to be in the nanometer scale. As expected, the surface area decreased and the particle size increased with raising the calcination temperature.

Fig. 3 shows the typical SEM micrographs of the $Ce_{0.8}Gd_{0.2}O_{1.9}$ powders at selected heating temperatures. The powders showed a foam-like morphology at 600 °C. This is probably due to the fact that the decomposition products of the organic residues in the complexes, such as CO, CO_2, H_2O and volatile hydrocarbon, did not escape easily from the resulting powders. By increasing the calcination temperature up to 1000 °C, the powders were made of blocky particles with an irregular shape, due to agglomeration and sintering taking place during the thermal treatment. The particle size ranged from submicron to larger than 1 μm. Fine powders with low agglomeration were obtained heating the complexes at 600 °C.

The pellet samples, prepared using the powders calcined at 600 °C, were sintered at 1500 °C for 5 h to ensure a high

Table 2
Density (% of the theoretical density) and activation energy of bulk, grain boundary, and total conductivities for $Ce_{0.9}Gd_{0.1}O_{1.95}$, $Ce_{0.85}Gd_{0.15}O_{1.925}$, and $Ce_{0.8}Gd_{0.2}O_{1.9}$ pellets sintered at 1500 °C.

Sample	Density (% theoretical)	Activation energy (eV)		
		Bulk	Grain boundary	Total conductivity
$Ce_{0.9}Gd_{0.1}O_{1.95}$	93	0.92	0.97	0.91
$Ce_{0.85}Gd_{0.15}O_{1.925}$	94	0.82	0.96	0.78
$Ce_{0.8}Gd_{0.2}O_{1.9}$	94	1.02	1.08	0.94

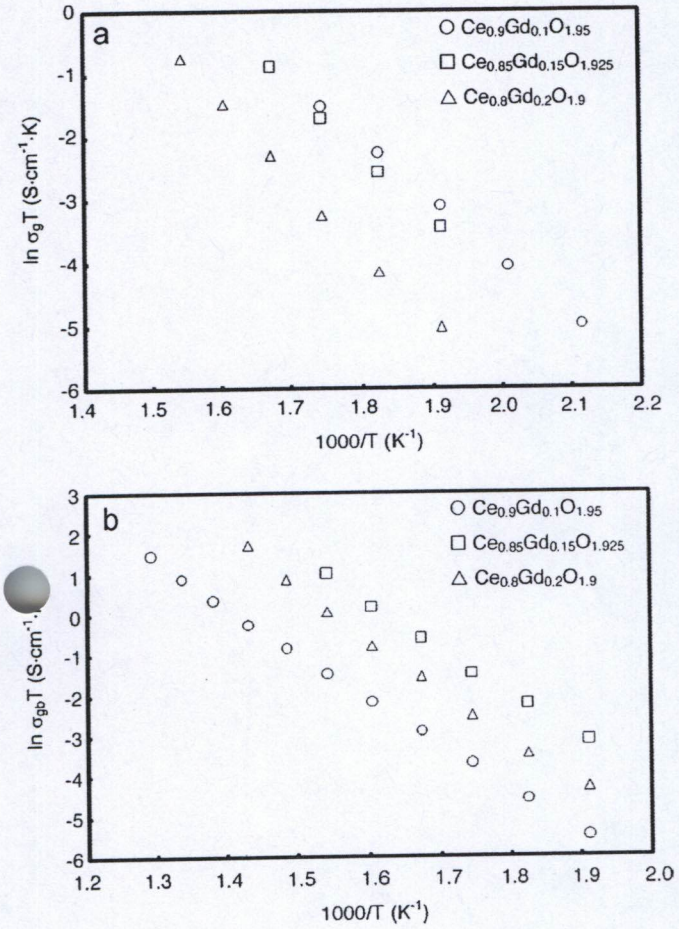

Fig. 5. Arrhenius plots of the (a) bulk and (b) grain boundary conductivity as a function of temperature for the $Ce_{0.9}Gd_{0.1}O_{1.95}$, $Ce_{0.85}Gd_{0.15}O_{1.925}$, and $Ce_{0.8}Gd_{0.2}O_{1.9}$ pellets.

density for electrical measurement. Phase identification was confirmed by XRD. The density of the pellets was more than 90% of the theoretical density before measurement, as shown in Table 2.

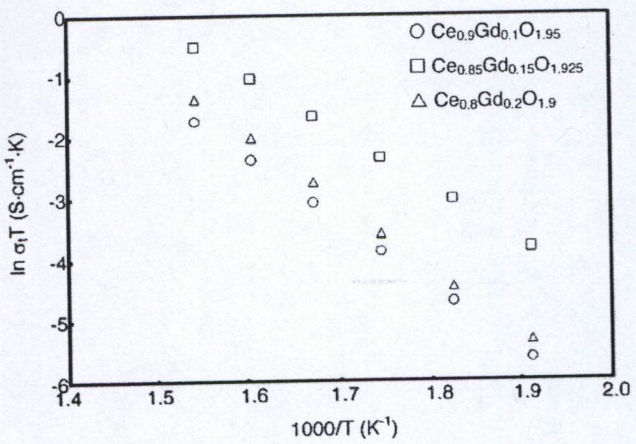

Fig. 6. Arrhenius plots of the total conductivity of the $Ce_{0.9}Gd_{0.1}O_{1.95}$, $Ce_{0.85}Gd_{0.15}O_{1.925}$ and $Ce_{0.8}Gd_{0.2}O_{1.9}$ pellets.

Fig. 4 shows the typical complex impedance plane plots of the $Ce_{0.85}Gd_{0.15}O_{1.925}$ pellet measured at (a) 250 °C, (b) 300 °C, (c) 400 °C, and (d) 600 °C. Two well-defined semicircular arcs were observed below 300 °C, which became one semiarc below 400 °C, accompanied by a spike at low frequencies. At higher temperatures, a single spike was observed. The same trend was observed for all the samples examined. The features in the impedance plots can be attributed to the contribution of the bulk (B) at high frequencies, the grain boundary (GB) at intermediate frequencies, and electrode

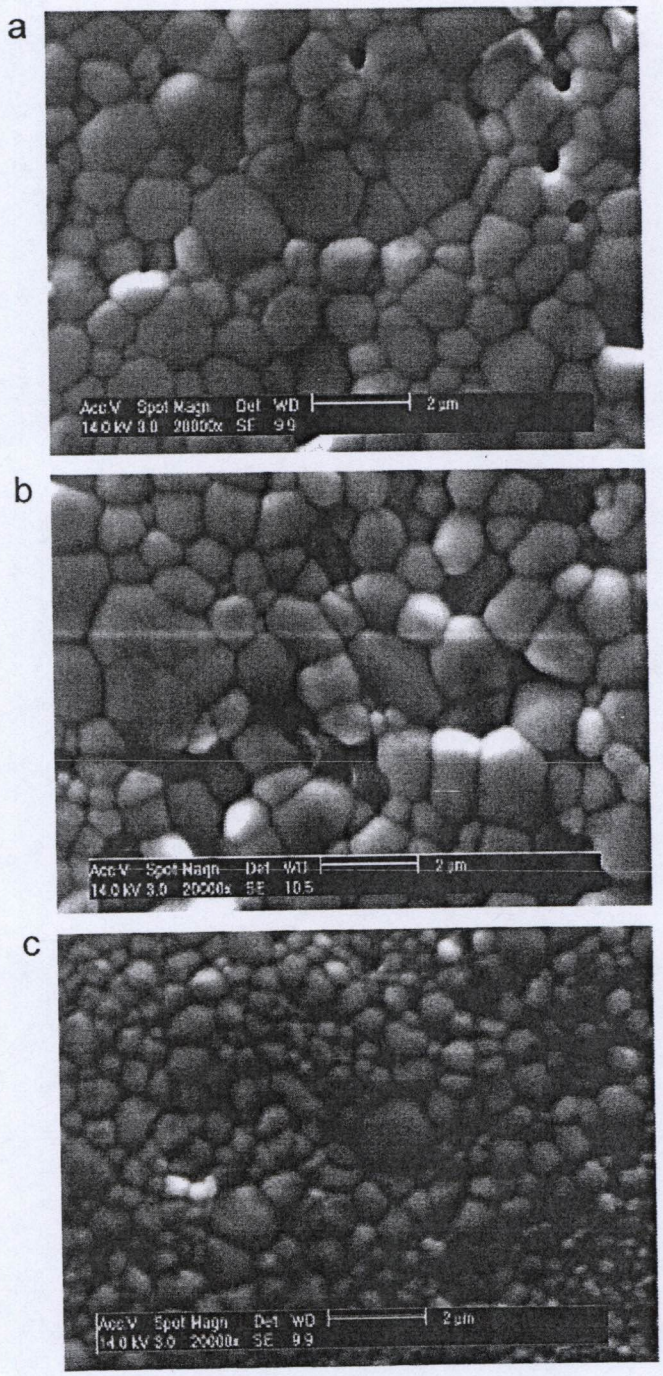

Fig. 7. SEM micrographs of (a) $Ce_{0.9}Gd_{0.1}O_{1.95}$, (b) $Ce_{0.85}Gd_{0.15}O_{1.925}$, and (c) $Ce_{0.8}Gd_{0.2}O_{1.9}$ pellets sintered at 1500 °C for 5 h.

polarization (E) at low frequencies, based on different relaxation frequency and capacitance values. The impedance behavior of $Ce_{1-x}Gd_xO_{2-(x/2)}$ ceramic pellets was similar to the trend usually observed for polycrystalline ceramic materials, as frequently documented in the literature [12].

Fig. 5(a) and (b) shows the Arrhenius plots of the apparent grain conductivity, σ_g, and the grain boundary conductivity, σ_{gb}, respectively, for $Ce_{0.9}Gd_{0.1}O_{1.95}$, $Ce_{0.85}Gd_{0.15}O_{1.925}$, and $Ce_{0.8}Gd_{0.2}O_{1.9}$ samples. The values were obtained from the EIS measurements.

It has been shown that oxygen-ion conductivity in rare earth (Re^{3+}) doped ceria can be represented by the following equation (2):

$$\sigma = \left(\frac{A}{T}\right) \exp\left(\frac{-E_a}{k_B T}\right) \quad (2)$$

One can observe that the bulk conductivity (σ_b) of the $Ce_{1-x}Gd_xO_{2-(x/2)}$ samples followed the order: $x = 0.1 > 0.15 > 0.2$, which is in agreement with the results documented in the relevant literature [6]. This is in line with expectations, because the increase in dopant concentration beyond $x = 0.1$ results in defect association, which in turn decreases the ionic conductivity. However, the grain boundary conductivity (σ_{gb}) of the $Ce_{1-x}Gd_xO_{2-(x/2)}$ samples followed the order: $x = 0.15 > 0.2 > 0.1$, which shows that the grain boundary conduction can be improved by an increase in dopant concentration above 10 mol%.

Fig. 6 shows the temperature dependence of the total conductivity, σ_t, for $Ce_{1-x}Gd_xO_{2-(x/2)}$ solid solutions. The total conductivity of the $Ce_{1-x}Gd_xO_{2-(x/2)}$ samples reached a maximum at $x = 0.15$. Usually, the maximum conductivity is believed to result from two divergent effects: (i) gadolinium substitution, which causes a significant increase in oxygen vacancy concentration and thus a rise in the ionic conductivity; (ii) the interaction between oxygen vacancies, which leads to a decrease in the mobility of vacancies and a subsequent decrease in the ionic conductivity. However, according to our study, it appears that the grain boundary conductivity determines the maximum in the total conductivity at $x = 0.15$. Moreover, Table 2 gives the activation energy values for all the samples, and $Ce_{0.85}Gd_{0.15}O_{1.925}$ showed the smallest activation energy values.

Fig. 7 shows the SEM micrographs of (a) $Ce_{0.9}Gd_{0.1}O_{1.95}$, (b) $Ce_{0.85}Gd_{0.15}O_{1.925}$, and (c) $Ce_{0.8}Gd_{0.2}O_{1.9}$ pellets sintered at 1500 °C. For $Ce_{0.85}Gd_{0.15}O_{1.925}$ and $Ce_{0.8}Gd_{0.2}O_{1.9}$, dense pellets were obtained, but the $Ce_{0.85}Gd_{0.15}O_{1.925}$ pellet showed larger grains corresponding to a smaller grain boundary volume, which might be the reason for the larger total conductivity observed for 15 mol% Gd doped ceria.

4. Conclusions

$Ce_{1-x}Gd_xO_{2-(x/2)}$ ($0.1 \leq x \leq 0.2$) solid solutions having a fluorite structure were prepared by the metal organic complex method. Ultrafine particles were formed. The small particle size of the doped ceria powders allowed the sintering of dense ceramic pellets at 1500 °C, which was smaller than 1600 °C, the temperature required to sinter the corresponding materials prepared by the conventional solid state method. The largest conductivity was found for the $x = 0.15$ Gd substituted ceria ($\sigma_{600\,°C} = 0.025$ S/cm).

Acknowledgments

The authors would like to thank The Center of Advanced Studies in Industrial Technology, Faculty of Engineering, Kasetsart University, Thailand, for their support. The authors also thank Mettler Toledo (Thailand) Limited for providing equipment on TGA/DTA analyzer, the Thailand Institute of Scientific and Technological Research (TISTR) for providing equipment on CIP, and the Thailand Institute of Nuclear Technology (TINT) for providing equipment on XRD and BET analysis. The authors would like to thank Asst. Prof. Dr. Duangrudee Chaysuwan, Assoc. Prof. Dr. Sutin Kuharuangrong, and Asst. Prof. Dr. Hathaikarn Manuspiya for their fruitful suggestions. The authors also thank Dr. Sumittra Charojrochkul, Dr. Pimpa Limthongkul and researchers from the National Metal and Materials Technology Center (MTEC), Thailand, for providing equipment for EIS measurements.

References

[1] A. Boudghene Stambouli, E. Traversa, Solid oxide fuel cells (SOFCs): a review of an environmentally clean and efficient source of energy, Renew. Sustain. Energy Rev. 6 (2002) 433–455.
[2] B.C.H. Steele, Material science and engineering: the enabling technology for the commercialisation of fuel cell systems, J. Mater. Sci. 36 (2001) 1053–1068.
[3] D.J.L. Brett, A. Atkinson, N.P. Brandon, S.J. Skinner, Intermediate temperature solid oxide fuel cells, Chem. Soc. Rev. 37 (2008) 1568–1578.
[4] H. Inaba, H. Tagawa, Ceria-based solid electrolytes, Solid State Ionics 83 (1996) 1–16.
[5] V. Esposito, E. Traversa, Design of electroceramics for solid oxide fuel cell applications: playing with ceria, J. Am. Ceram. Soc. 91 (2008) 1037–1051.
[6] B.C.H. Steele, Appraisal of $Ce_{1-y}Gd_yO_{2-y/2}$ electrolytes for IT-SOFC operation at 500 °C, Solid State Ionics 129 (2000) 95–110.
[7] F.Y. Wang, S. Chen, S. Cheng, Gd^{3+} and Sm^{3+} co-doped ceria based electrolytes for intermediate temperature solid oxide fuel cells, Electrochem. Commun. 6 (2004) 743–746.
[8] J. van Herle, D. Seneviratne, A.J. McEvoy, Lanthanide co-doping of solid electrolytes: AC conductivity behaviour, J. Eur. Ceram. Soc. 19 (1999) 837–841.
[9] J.M. Ralph, J. Przydatek, J.A. Kilner, T. Seguelong, Novel doping systems in ceria, Ber. Bunsen-Gesellschaft 101 (1997) 1403–1407.
[10] H. Yoshida, T. Inagaki, K. Miura, M. Inaba, Z. Ogumi, Density functional theory calculation on the effect of local structure of doped ceria on ionic conductivity, Solid State Ionics 160 (2003) 109–116.
[11] S. Kuharuangrong, Ionic conductivity of Sm, Gd, Dy and Er-doped ceria, J. Power Sources 171 (2007) 506–510.
[12] R.S. Torrens, N.M. Sammes, G.A. Tompsett, Characterisation of $(CeO_2)_{0.8}(GdO_{1.5})_{0.2}$ synthesised using various techniques, Solid State Ionics 111 (1998) 9–15.
[13] A.I.Y. Tok, L.H. Luo, F.Y.C. Boey, Carbonate co-precipitation of Gd_2O_3-doped CeO_2 solid solution nano-particles, Mater. Sci. Eng. A 383 (2004) 229–234.

[14] Y.P. Fu, S.B. Wen, C.H. Lu, Preparation and characterization of samaria-doped ceria electrolyte materials for solid oxide fuel cells, J. Am. Ceram. Soc. 91 (2008) 127–131.
[15] G. Ruifeng, M. Zongqiang, Sintering of $Ce_{0.8}Sm_{0.2}O_{1.9}$, J. Rare Earths 25 (2007) 364–367.
[16] S. Dikmen, P. Shuk, M. Greenblatt, H. Gomez, Hydrothermal synthesis and properties of $Ce_{1-x}Gd_xO_{2-\delta}$ solid solutions, Solid State Sci. 4 (2002) 585–590.
[17] R.O. Fuentes, R.T. Baker, Synthesis and properties of gadolinium-doped ceria solid solutions for IT-SOFC electrolytes, Int. J. Hydrogen Energy 33 (2008) 3480–3483.
[18] A. Laobuthee, S. Wongkasemjit, E. Traversa, R.M. Laine, $MgAl_2O_4$ spinel powders from oxide one pot synthesis (OOPS) process for ceramic humidity sensors, J. Eur. Ceram. Soc. 20 (2000) 91–97.

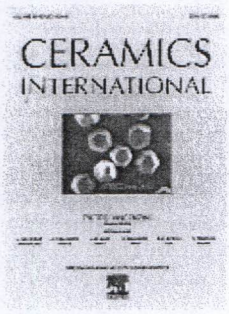

Ceramics International

Ceramics International primarily deals with the fundamental aspects of **ceramic science** and their application to the development of improved ceramic materials. The journal particularly encourages papers...

View full aims and scope

General Editor: P. Vincenzini
View full editorial board

Guide for Authors

Submit Your Paper

Track Your Paper

Order Journal

View Articles

Impact Factor: 1.789

5-Year Impact Factor: 1.968

Imprint: ELSEVIER

ISSN: 0272-8842

Related Publications

Cement and Concrete Research

Journal of the European Ceramic Society

Stay up-to-date

Register your interests and receive email alerts tailored to your needs

here to sign up

Follow us

Subscribe to RSS

Latest News

News

All Elsevier Materials Science journals now offer a new, free service to authors: AudioSlides These are brief, webcast-style presentations based on slides and audio that are shown next to the article on ScienceDirect.

VIEW ALL

Podcasts

Innovations in high precision thin film mechanical property characterization
13 September 2013

Advances in integrated EDS and EBSD microanalysis
5 September 2013

AFM-based infrared spectroscopy
30 August 2013

Bioelectronics Part 2
21 August 2013

VIEW ALL

Special Issues

Most Downloaded Articles

1. **Hydroxyapatite nanocomposites: Synthesis, sintering and mechanical properties**
M. Aminzare | A. Eskandari | ...

2. **Nanocomposite synthesis and characterization of Kesterite, Cu2ZnSnS4 (CZTS) for photovoltaic applications**
Elizabeth K. Michael | Danielle Norcini | ...

3. **Solvothermal synthesis of SnO2/graphene nanocomposites for supercapacitor application**
S.P. Lim | N.M. Huang | ...

VIEW ALL

Materials Science News

'Mechanical gears' seen in nature for the first time
13 September 2013

Toward a truly white organic LED
13 September 2013

Webinar: Innovations in high precision thin film mechanical property characterization
12 September 2013

Molecular pea-shooter
12 September 2013

VIEW ALL

Most Cited Articles

The 8th Asian Meeting on Electroceramics (AMEC-8)
Volume 39, Supplement 1 (2013)
ORDER NOW

The 7th Asian Meeting on Electroceramics (AMEC-7) in conjunction with the 7th Asian Meeting on Ferroelectricity (AMF-7)
Volume 38, Supplement 1 (2012)
ORDER NOW

The fifth Asian meeting on electroceramics (AMEC-5). Bangkok, Thailand. 10-14 December 2006
Volume 34, Number 4 (2008)
ORDER NOW

VIEW ALL

Ethanol sensor based on ZnO and Au-doped ZnO nanowires
Hongsith, N. | Viriyaworasakul, C. | ...

TiO2 optical coating layers for self-cleaning applications
Euvananont, C. | Junin, C. | ...

Combustion synthesis of high-performance Li4Ti5O12 for secondary Li-ion battery
Yuan, T. | Cai, R. | ...

VIEW ALL

Recent Articles

Calcium hydroxide-modified zinc polycarboxylate dental cements
Ali Zamanian | Mana Yasaei | ...

Ni-free, black ceramic pigments based on Co—Cr—Fe—Mn spinels: A reappraisal of crystal structure, colour and technological behaviour
Michele Dondi | Chiara Zanelli | ...

Effect of hafnium-incorporation on the microstructure and dielectric properties of cobalt ferrite ceramics
S. Wells | C.V. Ramana

VIEW ALL